Engineering Cytochromes for Photocatalysis: Biohybrid Assemblies for Light-Driven Dye Decoloration

Jessica H. van Wonderen,[a] Daisy L. Kent,[a] Mary E. G. Emmerson,[a] Samuel E. H. Piper,[a] Huijie Zhang,[b] Lars J. C. Jeuken,[c] Igor V. Sazanovich (Игорь Сазанович),[d] Michael Towrie,[d] Stephen R. Meech[a] and Julea N. Butt[a*]

[a] School of Chemistry and School of Biological Sciences, University of East Anglia, Norwich Research Park, Norwich, NR4 7TJ, UK

[b] School of New Energy, Nanjing University of Science and Technology, Jiangyin, Jiangsu 214443, China

[c] Leiden Institute of Chemistry, Leiden University, PO Box 9502, 2300 RA Leiden, The Netherlands

[d] Central Laser Facility, Research Complex at Harwell, STFC Rutherford Appleton Laboratory, Harwell Campus, OX11 0QX, UK

*Correspondence to:

Julea N. Butt

School of Biological Sciences, University of East Anglia, Norwich Research Park, Norwich, NR4 7TJ, UK

j.butt@uea.ac.uk

Abstract:

A major challenge in developing effective photocatalysts lies in engineering the efficient coupling of one-electron photochemistry with the multi-electron requirements of chemical transformations. Here we demonstrate biohybrid assemblies that achieve this key performance requirement by storing photoenergized electrons on multiple heme cofactors within the MtrC enzyme which catalyzes azo dye reduction. The biohybrid assemblies were created by site-selective labeling of MtrC with a Ru(II) (bipyridine)$_3$ photosensitizer dye. Photocatalytic azo dye reduction and decoloration occurred when these assemblies were irradiated in the presence of a sacrificial electron donor. Our Ru(II) (bipyridine)$_3$-MtrC biohybrid assemblies operate in a manner analogous to Ru(II) (bipyridine)$_3$-sensitized TiO_2 in the sense that photoenergized electrons accumulate in the MtrC heme chain rather than in the TiO_2 conduction band prior to driving reductive chemical transformations. We anticipate that decoration of the photosensitized MtrC protein with electrocatalysts (natural or synthetic) will enable the Ru(II) (bipyridine)$_3$-MtrC assemblies to drive a wide range of light-driven reductive transformations. Thus, MtrC provides a natural alternative to TiO_2 materials for which the production and disposal present significant environmental and energy impacts.

Keywords:

photocatalysis, cytochrome, bleaching, biohybrid, Ru(II) (bipyridine)$_3$, spectroscopy, azo dye

Highlights:

- a decaheme cytochrome stores photoenergized electrons to catalyze azo dye reduction
- the cytochrome is photosensitized site-selectively with Ru(II) (bipyridine)$_3$
- photocatalytic rates depend on azo dye reduction potential rather than structure

Graphical Abstract:

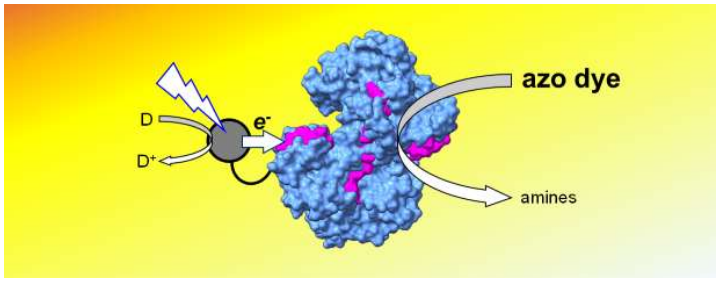

Introduction:

Recent years have seen rapid advances in the opportunities to impart proteins with new functionality through the introduction of non-biological components. Examples include the introduction of metals[1-3] to serve as novel catalytic centers and the genetic encoding of non-canonical amino acids.[4-7] There is also much interest in combining synthetic light-harvesting photosensitizers with enzymes to enable light-driven redox catalysis. In principle such biohybrid assemblies offer several advantages for photocatalysis when compared to purely synthetic or biological approaches.[8-12] For example, the superior photostability and broad band absorbance of a light-harvesting synthetic material can be combined with the ability of redox enzymes to perform valuable chemical transformations with selectivity and stereospecificity greater than synthetic equivalents where they exist.[13-16]

When developing photocatalytic biohybrid assemblies a major challenge lies in engineering the efficient coupling of one-electron photochemistry with the multi-electron requirements of chemical transformations. Thus, enzymes containing two or more redox cofactors are attractive as biohybrid components because they offer sites to store multiple photoenergized electrons (or holes). In this context bacterial multiheme cytochromes[17] are of considerable interest. These proteins contain three or more covalently bound redox active *c*-type heme cofactors. The hemes are arranged as a chain with neighboring sites in close proximity and this enables electron storage within, and transfer through, the proteins by complementary Fe(III) $\leftrightarrow$ Fe(II) transitions of adjacent sites.[17-21] In addition, at least one heme is positioned close to the protein surface to facilitate electron exchange with suitable redox partners. This has enabled light-driven reduction of multiheme cytochromes following their adsorption onto dye-sensitized TiO_2 nanoparticles[22, 23] and by diffusional encounter with photosensitizers including C-Dots[24] and dyes, both inorganic and organic.[23] Furthermore, multiheme cytochromes embedded in vesicular lipid bilayers enable electron transfer from external irradiated C-Dots to internalized enzymes and thus light-driven catalysis.[25, 26]

Multiheme cytochromes can also be photosensitized by site-selective labeling of surface cysteine residues with a well-characterized thiol-reactive Ru(II)(bipyridine)$_3$ dye.[27-33] Photoexcitation of that dye attached to oxidized, i.e., Fe(III)-heme containing, proteins is followed by oxidative quenching whereby the excited state dye injects the photoenergized electron into a nearby heme. That process produces charge separated states that are readily detected by transient absorbance spectroscopy through changes in the Soret- and Q-bands that

are diagnostic of the heme Fe(III) to Fe(II) conversion.[29-31] In the absence of sacrificial redox partners, the ground state is returned by charge recombination whereby the photoenergized electron moves from the heme chain back to the dye. The result is a futile redox cycle. However, when a sacrificial electron donor reduces the oxidized dye the photoenergized electrons become trapped on the hemes.[33, 34] Here we extend that state of the art by demonstrating that multiheme cytochromes photosensitized with a Ru(II) (bipyridine)$_3$ dye can deploy their photoenergized electrons for reductive photocatalysis, specifically, the light-driven reduction of azo dyes.

Azo dyes are characterized by having one or more azo group (-N=N-) attached to sp^2-hybridized carbons. Such dyes are widely used in print and textile industries due to their vibrant colors and stability but these properties also mean that the dyes are often associated with color pollution.[35] As a consequence, bleaching of azo dyes through reductive azo bond cleavage attracts much interest as a means to mitigate color pollution. Electrons for this four-electron reaction can be sourced directly from electrodes, photosensitized nanoparticles and microbial metabolism.[36-39] In an example of the latter process, species of *Shewanella* bacteria transfer excess electrons from central metabolism to the decaheme containing cytochrome MtrC that is located on the bacterial cell surface. Reduced MtrC then catalyzes azo dye reduction.[40-44] Thus, we chose to develop our photocatalytic biohybrid assembly using MtrC as an established catalyst for azo bond reduction.

In this work the MtrC protein was photosensitized by site-selective labeling of a surface cysteine residue with thiol reactive Ru(II) (bipyridine)$_3$ dye, Figure 1a. Photocatalytic azo dye reduction was observed when the biohybrid assemblies were irradiated in the presence of a sacrificial electron donor and our results are consistent with direct transfer of photoenergized electrons from MtrC hemes to azo dyes as illustrated in Figure 1b. Thus, we propose that photocatalysis is facilitated by the ability of dye-labeled MtrC to store photoenergized electrons within its heme wire in a manner analogous to the storing of photoenergized electrons in the conduction band of dye-sensitized TiO_2.[45, 46]

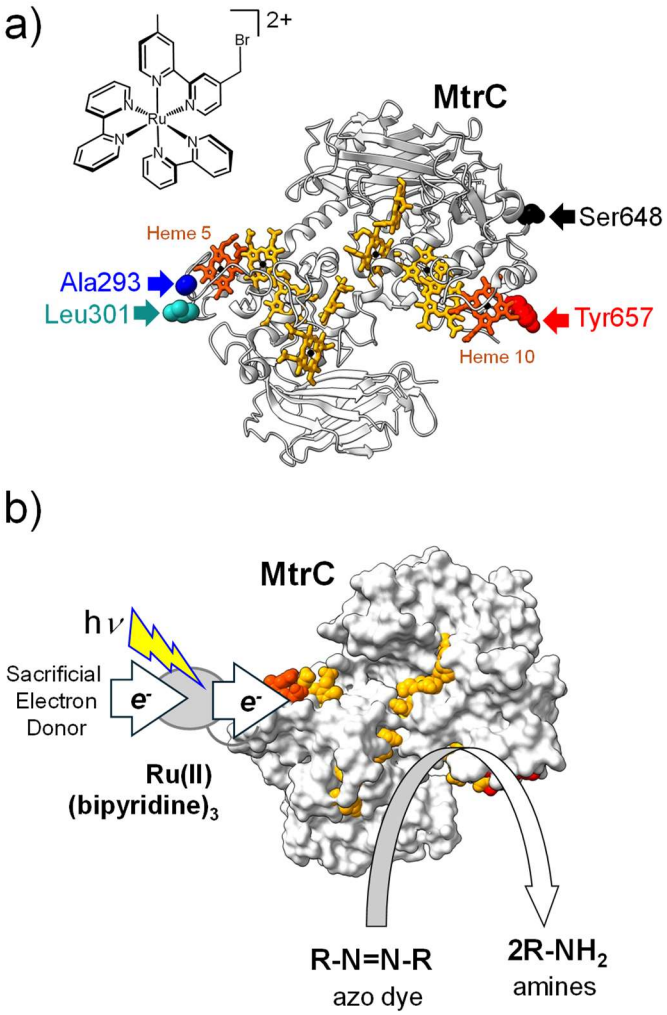

Figure 1. Overview of the systems studied in this work.

a) Structure of MtrC showing the hemes (orange/red) with $Fe^{2+/3+}$ (black). The highlighted surface residues 293 (blue), 301 (teal), 648 (black) and 657 (red) were replaced by cysteine for labeling with a thiol-reactive Ru(II)(bipyridine)$_3$ dye (inset).

b) Schematic of Ru-MtrC biohybrid assembly performing the photocatalytic reduction of azo dyes. Only productive electron transfer events are shown. (MtrC PDB ID: 4LM8)

Materials and Methods:

Protein Preparation and Ru-dye Labeling. Variant MtrC proteins were prepared as previously described.[31] The corresponding primers (Eurofins) are listed in **Table S1** and the plasmids and bacterial strains in **Table S2**. All MtrC variants carried a C-terminal Strep II tag to assist purification and were secreted from *S. oneidensis* MR-1 as soluble proteins. Previously described protocols were used for purification of the MtrC variants[47] and labeling with [Ru(4-bromomethyl-4'-methylbipyridine)(2,2'-bipyridine)$_2$](PF_6)$_2$ (HetCat, Switzerland).[30, 31, 33] In brief, Cys-directed labeling was enabled by exposing proteins to the disulfide reducing agent tris(2-carboxyethyl)phosphine (5 mM) for 30 min at room temperature to ensure the introduced Cys was present as thiol(ate). Protein was then recovered by exchange (3×) into 20 mM Tris-HCl, pH 7.5 using a centrifugal filter (5 kDa cut-off). Samples of 50 – 100 μM protein were incubated with a 2-fold molar excess of Ru(II) dye for 3 to 4 hours in the dark at room temperature. Purification of Ru(II)-dye labeled protein was by anion-exchange chromatography. Concentrations of protein and Ru(II) dye were quantified by electronic absorbance spectroscopy. For protein concentrations the measurements used air-equilibrated samples (all hemes in the oxidized Fe(III) state) and $\varepsilon_{410\,nm}$ = 1326 mM^{-1} cm^{-1} except for Y657C MtrC where $\varepsilon_{410\,nm}$ = 1389 mM^{-1} cm^{-1}.[31] For Ru(II) dye concentrations were calculated using $\varepsilon_{452\,nm}$ = 14.6 $mM^{-1}cm^{-1}$.[48]

Biochemical Analyses. Sample analysis by denaturing gel electrophoresis (SDS-PAGE) used mPAGE 4-20% Bis-Tris Precast gels (Merck) with proteins visualized by ReadyBlue Coomassie stain (Merck). Intact mass values were defined by liquid chromatography-mass spectrometry using positive mode electrospray ionization as described previously.[33] Masses for the purified proteins assumed that covalent modification by insertion of *c*-type heme introduced 615.17 g (mol heme)$^{-1}$.[49] Protein film electrochemistry was performed as previously described[31] using template stripped gold working electrodes with a self-assembled monolayer formed by overnight incubation in mixture of 0.8 mM 8-mercaptooctanoic acid (in water) and 0.2 mM 1-octanethiol (in ethanol).

Static and Time-Resolved Photoluminescence Spectroscopy. Data were recorded using an Edinburgh Instruments FS5-TCSPC spectrofluorometer with a picosecond pulsed diode laser (EPL series). Static excitation ($\lambda_{emission}$ = 625 nm) and emission ($\lambda_{excitation}$ = 455 nm) spectra were recorded with a slit width of 3 nm and dwell time of 0.2 s. Time-resolved photoluminescence decay used excitation at 485 nm with data collection for 20 min with a time

window of 2 ms (500 kHz). Anaerobic samples containing 0.7 μM MtrC, Ru-MtrC, or Ru(II)(4-bromomethyl-4'-methylbipyridine)(bipyridine)$_2$(PF_6)$_2$ were prepared in 20 mM Tris-HCl, 100 mM NaCl, pH 8.5 in sealed 1 mL quartz fluorescence cuvettes. Data were analyzed using Fluoracle software. To remove the fast component observed in buffer-electrolyte and unlabeled protein samples, the corresponding datasets were subtracted from those for the Ru(II) dye labeled proteins before analysis to define decay lifetimes (τ). Decay lifetimes are reported for the best fit with the smallest number of parameters, Eq. 1, with B as amplitude.

$$Intensity\ (t) = \sum_{i=1}^{n} B_i exp\left\{-\frac{t}{\tau_i}\right\} \qquad \text{(Eq. 1)}$$

Transient Absorbance Spectroscopy. Experiments were performed using the Time-Resolved Multiple-Probe Spectroscopy (TRMPS) facility at the Central Laser Facility of the Rutherford Appleton Laboratory.[30] Data collection and analysis was essentially as described previously for Ru657-MtrC.[31] Samples were prepared in anaerobic 20 mM Tris-HCl, 100 mM NaCl, pH 8.5. Spectral changes in the region of 470 – 650 nm used protein concentrations of ~150 μM. For spectral changes in the region of 350 – 440 nm the protein concentration was ~5 μM. These concentrations were selected to ensure equally good signal-to-noise ratios for quantitative analysis at each wavelength of interest noting that less intense features appear in the 470 – 650 nm region. An appropriate cut-off optical filter was used to block the scattered 457 nm excitation light (short-pass filter when probing 350-440 nm region and long-pass filter when probing 470-650 nm region). Measurements were performed in pairs, first Ru-MtrC and then the corresponding unlabeled protein (MtrC) at a similar concentration. Spectra for the unlabeled proteins were subtracted from those of the Ru(II) dye labeled proteins to give the effects of Ru dye excitation only. The resulting data were analyzed to provide the population of the charge separated Ru^+-$MtrC^-$ state as previously described.[31] In brief, the Q-band features were analyzed to calculate the concentration of Fe^{2+} which corresponds to the concentration of Ru^+-$MtrC^-$. The initial concentration of Ru(II) dye triplet excited state was calculated from the absorbance at 369 nm before charge separation occurs (1-5 ps). The population of Ru^+-$MtrC^-$ was calculated by assuming decay of the excited state dye occurs only by oxidative quenching. This assumption was verified because the transient populations[31] of the photo-excited state, charge separated state and ground state summed to 1 over the respective time courses, Figure S1.

Cumulative Photoreduction and Azo Dye Reduction. Spectra were recorded in 1 cm path length cuvettes in a Biochrom WPA Biowave II Diode-array spectrophotometer placed in a N_2-

filled chamber (Belle Technology, atmospheric O_2 < 5 ppm). An Omega Optical 475RB Notch filter prevented photoexcitation by the spectrophotometer. Photoreduction was driven by a Thorlabs mounted LED (λ_{max} = 450 nm) equipped with a collimator adapter. Samples were irradiated continuously from above and the excitation intensity at the sample was 110 W m^{-2} (0.42 mE m^{-2} s^{-1}) as determined by potassium ferrioxalate actinometry. Unless stated otherwise, experiments were performed in anaerobic 500 mM EDTA, 20 mM Tris-HCl, 100 mM NaCl, pH 8.5 prepared with Milli-Q water (resistivity > 18.2 MΩ cm)**.**

To measure cumulative photoreduction, the absorbance prior to irradiation was confirmed as that indicative of fully oxidized protein (0% reduced heme). Following irradiation, the absorbance of fully reduced protein (100% reduced heme) was obtained by addition of an excess of the chemical reductant sodium dithionite. The percentage of photoreduced hemes was quantified using the difference in absorbance at 552 nm and the 561 nm isosbestic wavelength.

To measure azo dye reduction, the following were used as provided; Amaranth (Sigma), Methyl Orange (Sigma-Aldrich) and Reactive Black 5 (Sigma-Aldrich). Stock solutions (approximately 2.5 mM) were prepared in water. Concentrations were quantified using the Beer-Lambert law with the following extinction coefficients: Amaranth $\varepsilon_{520\ nm}$ = 22.6 mM^{-1} cm^{-1},[50] Methyl Orange $\varepsilon_{464\ nm}$ = 20 mM^{-1} cm^{-1},[51] Reactive Black 5 $\varepsilon_{600\ nm}$ = 20 mM^{-1} cm^{-1}.[52] To quantify photoreduction of Amaranth and Methyl Orange, since the notch filter prevented analysis at 464 and 520 nm, extinction coefficients of $\varepsilon_{565\ nm}$ = 0.76 mM^{-1} cm^{-1} and $\varepsilon_{565\ nm}$ = 12.4 mM^{-1} cm^{-1}, respectively, were used. Those values were calculated from inspection of the full spectrum of each dye.

Cyclic Voltammetry of Azo Dyes. Experiments employed a previously described[53] three-electrode cell inside a Faraday cage within a N_2-filled chamber (atmospheric O_2 < 5 ppm). The graphite 'edge' working electrode was rotated at 500 rpm during measurements. The counter electrode was a platinum wire and the reference electrode Ag/AgCl in saturated KCl. Measured values were converted to values *versus* SHE by the addition of 197 mV. Measurements were performed in 20 mM Tris-HCl, 100 mM NaCl, pH 8.5.

Results and Discussion:

Four Ru(II) (bipyridine)$_3$ dye labeled MtrC assemblies, termed Ru-MtrC hereafter, were studied in this work. The following sections describe their biochemical characterization and photochemistry in the absence of sacrificial electron donors. Then data from irradiating the Ru-MtrC assemblies with a sacrificial electron donor are presented to quantify cumulative photoreduction and photocatalytic azo dye reduction. Here some relevant properties of the biohybrid assemblies are provided as context for those analyses.

The hemes of MtrC form a chain extending approximately 65 Å and spanning the protein structure, Figure 1a. Those hemes are numbered according to the order in which their CxxCH attachment sites appear in the protein sequence with the consequence that the chain is terminated at one end by Heme 5 and at the opposite end by Heme 10. Ru-MtrC assemblies having the photosensitizer positioned closest to Heme 5 were prepared from protein having either Ala293 or Leu301 replaced by Cys, Figure 1a. The closest distance between the sulfur of the Ru(II) dye labeled cysteine and the conjugated ring of Heme 5 is predicted as 14.6 Å for Ru293-MtrC and 11.7 Å Ru301-MtrC using the FoldX plug-in within YASARA.[54-57] Ru-MtrC assemblies having the photosensitizer positioned closest to Heme 10 were prepared from protein having either Ser648 or Tyr657 replaced by Cys, Figure 1a. In the following text the Ru(II) dye labeled proteins are termed RuXXX-MtrC where XXX denotes the Cys labeling site. There is no reaction of the Ru(II) dye with MtrC lacking surface mutations.[31]

Biochemical Characterization of Ru-MtrC Biohybrids. Electronic absorbance spectroscopy of the air equilibrated Ru-MtrC samples was consistent with a 1:1 stoichiometry of Ru(II) dye:MtrC protein. As illustrated for Ru293-MtrC in Figure 2a, the corresponding spectra are dominated by a Soret peak ($\lambda_{max} \approx 410$ nm) accompanied by a smaller αβ-band around 540 nm that arise from low-spin Fe(III)-containing heme cofactors.[58] Absorbance by the Ru(II) dye is seen at UV wavelengths ($\lambda_{max} \approx 288$ nm) with a weaker feature at visible wavelengths ($\lambda_{max} \approx$ 460 nm), Figure 2b. Subtracting the absorbance of unlabeled protein from that of Ru-MtrC reveals a difference spectrum with features highly similar to the absorbance of Ru(II) dye, Figure 2b. Using the Beer-Lambert Law to calculate the concentration of Ru(II) dye and of MtrC indicates essentially 1:1 dye-labeling of MtrC. Similar behavior was displayed by the other Ru-MtrC proteins, Figure S2.

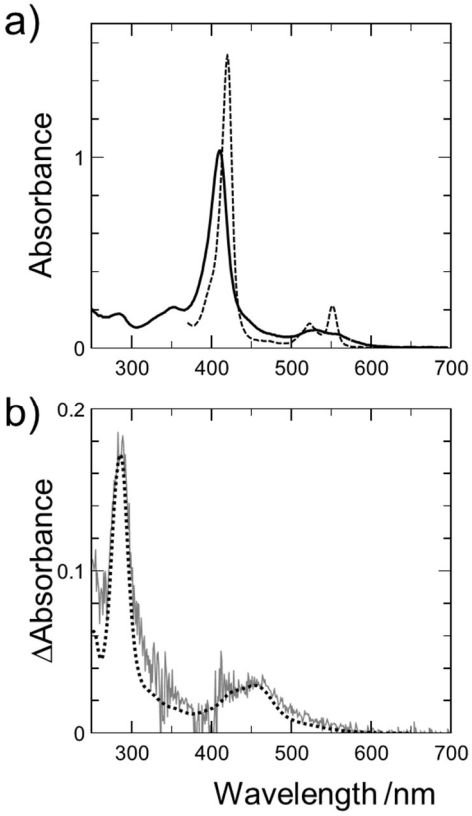

Figure 2. Electronic absorbance spectra of Ru293-MtrC and the unreacted Ru(II) dye.

a) Electronic absorbance of Ru293-MtrC (0.8 μM) in the oxidized, all-Fe(III) heme, state (continuous line) and reduced, all Fe(II) heme, state (dashed line). Oxidized protein is air equilibrated. Reduced protein produced by addition of excess sodium dithionite which dominates the absorbance below 370 nm such that the corresponding region of the spectrum is not shown.

b) Absorbance difference spectrum Ru293-MtrC *minus* Cys293-MtrC (gray line) for both proteins in the oxidized state. Spectrum of unreacted Ru(II) dye (black dotted line) with absorbance normalized to the difference spectrum at 288 nm.

Samples in 20 mM Tris-HCl, 100 mM NaCl, pH 8.5.

Integrity of the Ru-MtrC proteins was corroborated by denaturing gel electrophoresis, Figure S3, and liquid chromatography-mass spectrometry, Figure S4. Both methods revealed homogeneous samples and the mass spectrometry resolved masses in good agreement with those predicted for the corresponding MtrC peptides with 10 *c*-type hemes and a single Ru(II)(4-methyl-4'-methylbipyridine)(2,2'-bipyridine)$_2$, Table S3. Taken together, the results from electrophoresis, mass spectrometry and electronic absorbance spectroscopy are indicative of samples containing the desired Ru-MtrC proteins at greater than 95% purity.

Redox activity of the hemes in Ru-MtrC proteins was confirmed by electronic absorbance spectroscopy following addition of the chemical reductant sodium dithionite, Figure 2a, Figure S3. The reductant induced a shift of the Soret band to longer wavelength ($\lambda_{max} \approx 420$ nm). Sharp peaks also appeared in the α/β region centered at 523 and 552 nm. These spectral changes indicate the formation of low-spin, Fe(II)-containing hemes and reproduce behavior displayed by the native MtrC protein.[47, 58] A complementary description of redox activity in the Ru-MtrC proteins was provided by protein film cyclic voltammetry following their adsorption on surface-modified gold electrodes. Peaks for reduction and oxidation show reversible redox chemistry over a similar potential window (approximately 0 to -400 mV versus SHE) for all four proteins, Figure S5. The current-potential profiles are similar to each other and those of MtrC without surface mutations when allowing for small differences in the current-potential profiles that can be attributed to small differences in the baseline response from each electrode.[58] Thus, we consider that the four Ru-MtrC proteins have structures highly similar to that resolved[59] for MtrC having the native residues in surface locations 293, 301, 648 and 657. Specifically, the ten hemes in each Ru-MtrC protein are considered to have His/His axial ligation and the spatial arrangement illustrated in Figure 1a for the wild-type MtrC protein.

Photochemistry of Ru-MtrC Biohybrids in the Absence of Sacrificial Redox Partners. Photoluminescence and transient absorbance spectroscopies were used to gain insight into the consequences of irradiating Ru-MtrC proteins into the Ru(II) dye metal-to-ligand charge transfer band, Figure 3a process ①. For the unreacted Ru(II) dye, such irradiation forms a long lived triplet excited state that relaxes back to the ground state by emitting orange-red light, Figure 3 process ②. The emission and excitation spectra of the Ru-MtrC proteins had similar shapes to those of the unreacted Ru(II) dye, Figure 4a. However, spectral intensity for the labeled proteins was lower than that of the unreacted dye and decreased in the order Ru648-MtrC > Ru293-MtrC ≈ Ru301-MtrC > Ru657-MtrC. Time resolved photoluminescence spectroscopy showed faster decay for photoexcited Ru-MtrC systems than for the unreacted Ru(II) dye, Figure 4b.

The luminescent properties of the Ru-MtrC proteins are unlikely to arise from photoluminescence quenching of the photoexcited dye by Förster resonance energy transfer because there is poor spectral overlap of the Ru(II) dye emission and heme absorbance. Thus, the most reasonable interpretation is that photoluminescence quenching in the irradiated Ru-MtrC proteins arises from charge separation, Figure 3a process ③, whereby the photoexcited dye is quenched by injecting an electron into oxidized MtrC. For each Ru-MtrC protein, quenching is well-described by a multi-exponential fit with the contributions and lifetimes presented in Table 1. Based on previous work,[30, 31] the different contributions are most reasonably attributed to the presence of multiple Ru(II) dye conformers that are unable to exchange on the experimental timescale and that have different charge separation rates. Each of these conformers would place a bipyridyl ligand of the Ru(II) dye within 10 Å of the conjugated ring of the neighboring heme, Heme 5 or 10, to allow for charge injection into that heme on the pico-second to nano-second timescale. Since the photoluminescence decay properties are dependent on the labeling site, Table 1, it can be concluded that the structures and populations of these conformers are determined by the location of the Ru(II) dye attachment site.

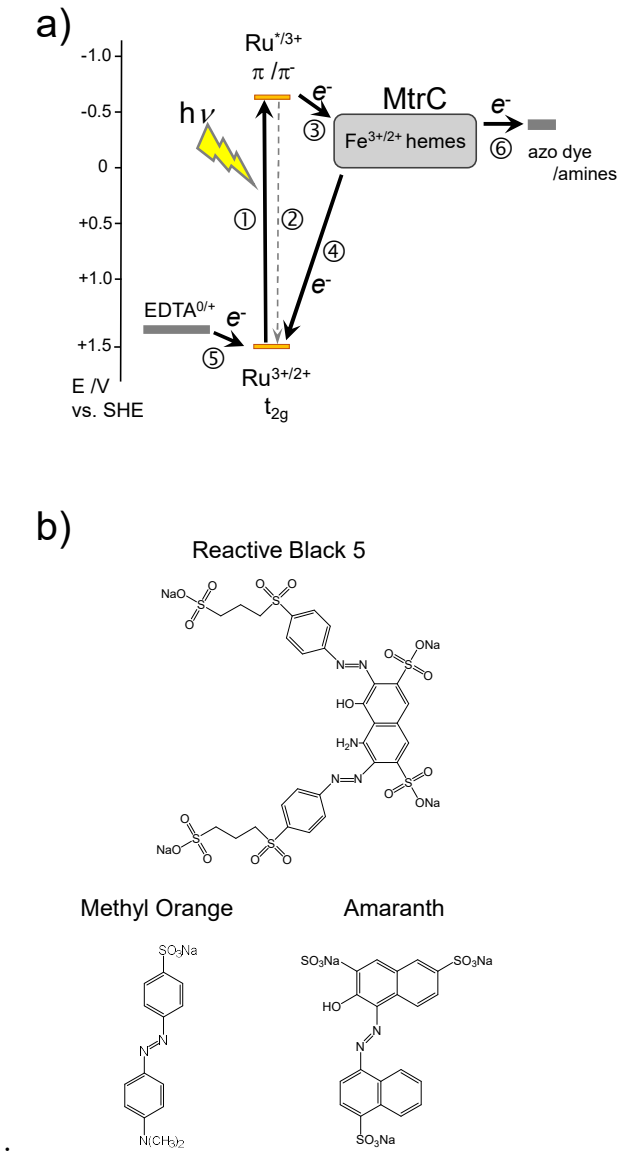

Figure 3. Photochemistry and azo dyes studied in this work.

a) Schematic energy level diagram for azo dye reduction by irradiated Ru-MtrC biohybrid assemblies with EDTA as sacrificial electron donor. An upper limit on the azo dye reduction potentials relevant to this study is indicated, see text for details.

b) Azo dye structures.

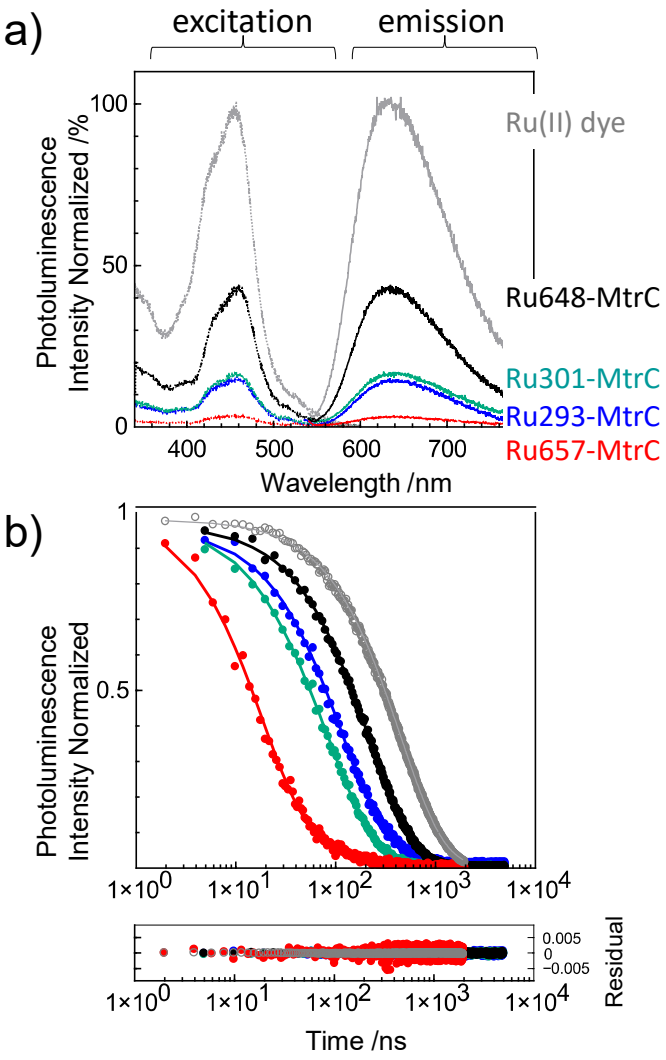

Figure 4. Photoluminescence properties of the Ru-MtrC proteins.

a) Excitation (λ_{em} = 625 nm) and emission (λ_{ex} = 455 nm) spectra for the unreacted Ru(II) dye and Ru-MtrC proteins as indicated. Intensity normalized to the maximum displayed by the unreacted Ru(II) dye.

b) Time-resolved photoluminescence decay (circles) for excitation at 485 nm (500 kHz) with emission measured at 625 nm. Ru293-MtrC (blue), Ru301-MtrC (teal), Ru648-MtrC (black), Ru657-MtrC (red) and Ru(II) dye (gray). Fits (lines) have the parameters of Table 1. Residuals below. Data for Ru657-MtrC and Ru(II) dye redrawn from van Wonderen et al PNAS 2021.[31]

Samples were 0.7 μM Ru-MtrC or Ru(II) dye in anaerobic 20 mM Tris-HCl, 100 mM NaCl, pH 8.5.

Table 1. Photoluminescence decay properties of Ru-MtrC proteins.[a]

	Fit parameters				
	τ_a /ns (% contribution)	τ_b /ns (% contribution)	Chi^2	Mean fluorescence lifetime /ns	Ref.
Ru293-MtrC	99 ± 3 (82%)	291 ± 10 (18%)	1.07	134	This work
Ru301-MtrC	36 ± 6 (36%)	101 ± 2 (63%)	1.13	77	This work
Ru648-MtrC	146 ± 19 (27%)	253 ± 6 (73%)	0.98	224	This work
Ru657-MtrC	18 ± 0.5 (89%)	121 ± 2 (11%)	1.10	29	[31]

[a] Data of Figure 4b, fit to two exponentials with each contribution attributed to a different conformer, see text for details. Mean fluorescence lifetime is amplitude weighted. Decay of the unreacted Ru(II) dye under equivalent conditions is described by a single exponential with lifetime 460 ± 2 ns (Chi^2 = 1.02).

Direct evidence for quenching of the photoexcited dye through formation of a charge separated state, specifically Ru^{+}-$MtrC^{-}$, was provided by transient absorbance spectroscopy. The resulting difference spectra (post-excitation minus pre-excitation) are reported in Figure 5 where chromophores with transiently depleted populations give negative features while those with transiently increased populations give positive features. Immediately after excitation the peak at 369 nm and broad positive feature above approximately 580 nm arise from absorbance by the dye triplet excited state, formally $[Ru(III)(\text{ bipyridine})_2(\text{bipyridine}^{-})]^{2+}$.[60-62] Over time, the disappearance of features from the photoexcited dye is accompanied by the appearance of peaks at 419 and 552 nm due to the presence of Fe(II) heme in the charge separated state. Depletion of the ground-state Ru(II)-dye population is evident in the broad trough between ~400 and 500 nm, and this feature recovers over time as the system returns to the ground state by charge recombination, Figure 3a process ④, as determined by the energetics of the system, Figure 3a. We note that in these experiments the Ru(II) dye metal-to-ligand charge transfer band was excited by pulsed irradiation at 457 nm which also results in direct excitation of the hemes. A previously described protocol[31] subtracted transient absorbance of Cys-MtrC from that of the corresponding Ru-MtrC to provide the data presented in Figure 5 that describes only the photochemistry associated with excitation of the Ru(II) dye and shown schematically in Figure 3a.

The sharp Q-band feature centered at 552 nm in the transient absorbance spectroscopy arising from Fe(II) heme was used to define the evolution of the Ru^{+}-$MtrC^{-}$ charge separated state for each Ru-MtrC assembly, Figure 6. That evolution is clearly dependent on the location of the Ru(II) dye labeling site. Such behavior is expected since for each protein there are contributions from multiple Ru(II) dye conformers with different rates of charge separation, Table 1, and most likely different rates of charge recombination. There is also the possibility of heme-to-heme electron transfer within the charge separated Ru^{+}-$MtrC^{-}$ states and where the dynamics following injection into Heme 5 will be different from those following injection into Heme 10 due to the different microscopic reduction potentials, spatial separation and electronic coupling of the relevant heme pairs.[31, 63] For Ru657-MtrC, a previous study[31] provided a quantitative description of the corresponding photocycle that was in excellent agreement with independent predictions of the behavior using state-of-the-art methodologies in density functional theory and molecular dynamics calculations. However, such analysis is beyond the needs of the present study since the population and persistence of the Ru^{+}-$MtrC^{-}$ charge separated states will determine the photocatalytic performance of the corresponding system.

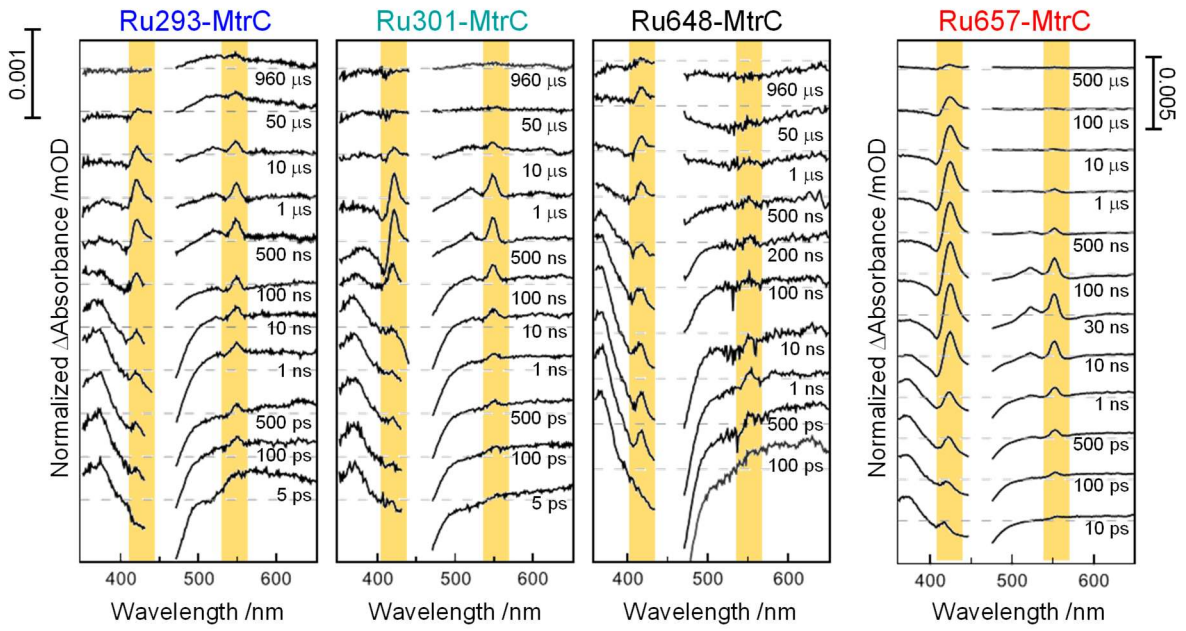

Figure 5. Transient absorbance spectra of Ru-MtrC proteins as indicated.

Difference absorbance spectra (post- minus pre-excitation) for the indicated times after irradiation. Yellow panels highlight spectral regions indicative of heme oxidation state. Pulsed irradiation was at 457 nm and contributions from electronically excited hemes are removed as described previously.[31] Samples contained Ru-MtrC (5 µM for measurements <440 nm, ≈150 µM for measurements >470 nm) in anaerobic 20 mM Tris-HCl, 100 mM NaCl, pH 8.5.

Data for Ru657-MtrC redrawn from van Wonderen et al PNAS 2021.[31]

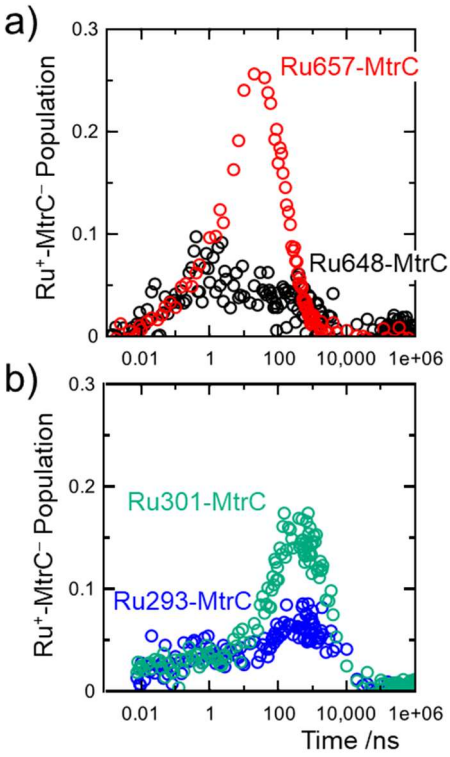

Figure 6. Population of the Ru^{+}-MtrC^{-} charge separated states determined by transient absorbance spectroscopy.

a) MtrC proteins labeled with Ru(II) dye closest to Heme 10 at residue 648 and 657 as indicated.

b) MtrC proteins labeled with Ru(II) dye closest to Heme 5 at residue 293 and 301 as indicated.

Measurement conditions as for Figure 5. Data for Ru657-MtrC redrawn from van Wonderen et al PNAS 2021.[31]

The Ru^{+}-$MtrC^{-}$ charge separated state is visible just beyond 1 μs, Figure 6a, for Ru648-MtrC and Ru657-MtrC that place the Ru(II) dye closest to Heme 10. However, the Ru^{+}-$MtrC^{-}$ charge separated state persists slightly beyond 10 μs, Figure 6b, for Ru293-MtrC and Ru301-MtrC that place the Ru(II) dye closest to Heme 5. Despite the caveats above it could be that these behaviors have their origin in the different microscopic reduction potentials predicted for Heme 10 (-137 mV) and Heme 5 (+46 mV).[63] Thus, there is less driving force, Figure 3a, for charge separation at Heme 10 than Heme 5 and greater driving force for charge recombination at Heme 10 than Heme 5. However, such simple reasoning fails to account for the trend in maximum Ru^{+}-$MtrC^{-}$ population. The maximum population decreases in the order Ru657-MtrC > Ru301-MtrC > Ru648-MtrC ≈ Ru293-MtrC, Figure 6.

***Cumulative Photoreduction of Ru-MtrC Biohybrids*:** Experiments to assess the ability of the Ru-MtrC proteins to accumulate photoenergized electrons employed continuous irradiation into the Ru(II) dye metal-to-ligand charge transfer band of anaerobic solutions containing ethylenediaminetetraacetic acid (EDTA) as sacrificial electron donor.[33, 34] Electronic absorbance spectra recorded over one hour of irradiation showed that features arising from oxidized Fe(III)-hemes were gradually replaced by features indicative of reduced Fe(II)-hemes as illustrated for Ru657-MtrC in Figure 7a. Specifically, there was a red shift and increase of intensity in the Soret band and the appearance of lower intensity peaks at 520 and 552 nm. Comparison of these spectral changes to those produced by complete reduction of the ten MtrC hemes on addition of the chemical reductant sodium dithionite allowed the percentage of photoreduced heme to be calculated using the difference in absorbance at 552 nm and the 561 nm isosbestic wavelength. That analysis showed that 1 hour irradiation resulted in the reduction of approximately 9 hemes per MtrC protein, Figure 7b. The reduced hemes will be those having the more positive reduction potentials. However, the oxidation state of individual hemes cannot be distinguished since the optical properties of the ten hemes, all of which have His/His axial iron ligands, cannot be distinguished.[31]

When the irradiation was removed there were no further changes to the spectra over a period of 5 min. Separate experiments provided no evidence for heme reduction in the absence of light, EDTA, or the Ru(II) dye, Figure 7b gray symbols. The most reasonable interpretation of the data is that following formation of a Ru^{+}-$MtrC^{-}$ charge separated state, a photoenergized electron is trapped in the MtrC heme chain when the oxidized 'Ru^{+}' dye is returned to its

ground state through reduction by EDTA as sacrificial electron donor, Figure 3a process ⑤. Subsequent absorption of additional photons enables trapping of additional electrons in MtrC such that almost complete reduction of the photosensitized MtrC protein is observed after 1 hour irradiation.

Parallel experiments provided similar evidence for cumulative photoreduction of the Ru293-, Ru301- and Ru648-MtrC biohybrid assemblies and those time courses are compared in Figure 7b. It is notable that for all assemblies, several minutes irradiation is needed to produce > 50% photoreduction and that experiments with lower concentrations of EDTA showed slower initial rates of cumulative reduction, e.g., Figure 7a insert. These findings are consistent with oxidation of EDTA by the charge separated Ru^{+}-$MtrC^{-}$ states, Figure 3a process ⑤, presenting a rate defining event in cumulative photoreduction. Also apparent is that that the initial rate of Ru648-MtrC cumulative photoreduction is significantly less than that of the other proteins. We attribute this behavior to the properties of the corresponding charge separated state which for Ru648-MtrC is maximally populated to a lesser extent and at shorter times than those of the other biohybrid assemblies, Figure 6.

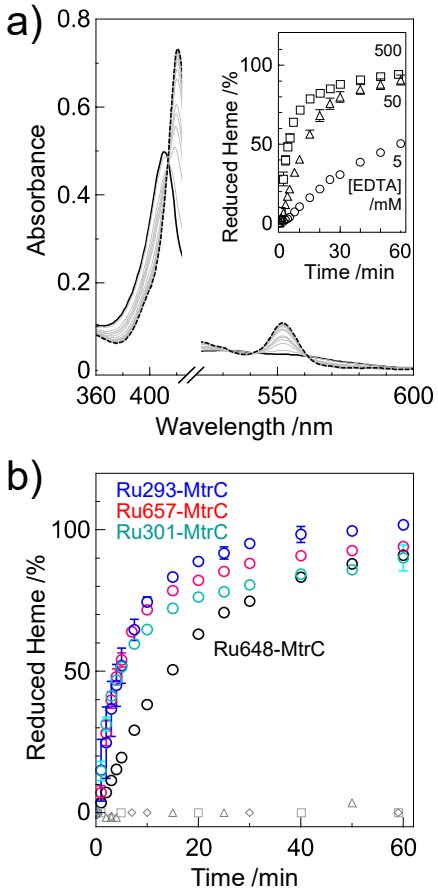

Figure 7. Cumulative photoreduction of Ru-MtrC proteins.

a) Representative electronic absorbance of Ru657-MtrC before (continuous black), during (gray), and after (dashed black) 60 min irradiation in 500 mM EDTA. Absorbance values between 430 and 520 nm are absent due to the use of a notch filter (Omega Optical 475RB) to prevent photoexcitation by the spectrophotometer. Inset: time courses for photoreduction of Ru657-MtrC at 5, 50 and 500 mM EDTA as indicated. Measurements in anaerobic 20 mM Tris-HCl, 100 mM NaCl, pH 8.5 at ambient temperature.

b) Photoreduction time courses (circles) for Ru-MtrC proteins as indicated. Samples (0.35 μM protein) in anaerobic 500 mM EDTA, 20 mM Tris-HCl, 100 mM NaCl, pH 8.5 at ambient temperature with irradiation at 450 nm, intensity 110 W m^{-2} at the sample. Gray symbols are for control experiments performed as above except using Ru657-MtrC in the absence of light (squares), without EDTA (diamonds) and with Ru657-MtrC replaced by the corresponding unlabeled protein, Y657C-MtrC (triangles).

***Photocatalytic Azo Dye Reduction by Ru-MtrC Biohybrids*:** Having demonstrated accumulation of photoenergized electrons in the MtrC heme chain, a final series of experiments assessed the ability of those electrons to catalyze the reductive decoloration of azo dyes through the four-electron reductive cleavage of the azo group to its corresponding amines. Experiments were performed with Ru-MtrC at concentrations of approximately 0.3 μM and an excess (at least 40-fold) of azo dye to enable catalytic photoreduction to be distinguished from a process where Ru-MtrC is a stoichiometric reductant. The azo dyes selected for study were Reactive Black 5, Methyl Orange and Amaranth for which the structures are illustrated in Figure 3b. We selected two biohybrid assemblies for study, namely, Ru301-MtrC and Ru657-MtrC. These assemblies positioned the photosensitizer at either end of the MtrC heme chain, Figure 1a, and produced the maximum population of the charge separated state for that labeling site, Figure 6. Ru301-MtrC and Ru657-MtrC behaved similarly in preliminary experiments. Thus, we chose one or other protein for subsequent and more detailed quantitative studies as described below.

Reductive decoloration of Reactive Black 5 is evidenced by a decrease of its prominent absorbance at 600 nm when irradiated, for example, in the presence of Ru657-MtrC and EDTA Figure 8a. The amount of Reactive Black 5 reduced during 1 hour irradiation was slightly more for Ru657-MtrC than for Ru301-MtrC, Figure 8b and S6, and in both cases 5-fold more than the reduction in parallel experiments without the biohybrids, Figure 8b and S6. Bleaching of Reactive Black 5 in experiments that omitted either EDTA or light occurred at rates that were typically 10-fold lower than in the presence of Ru-MtrC, Figure S7. Similarly low rates of bleaching were also measured during irradiation with EDTA and including unreacted Ru(II) dye, or unlabeled MtrC, in place of Ru-MtrC. Thus, there is no evidence for direct transfer of photoenergized electrons from the Ru(II) dye or unlabeled MtrC to the azo dye. Taken together, the data are consistent with the Ru-MtrC biohybrid assemblies accelerating the light-driven reduction of Reactive Black 5. With just 0.3 μM Ru-MtrC driving the reduction of > 5 μM Reactive Black 5, Figure 8b, we conclude that the biohybrid is acting as a photocatalyst.

Our proposed mechanism for photocatalysis is illustrated schematically in Figures 1b and 3a. Photoexcited Ru(II) dye injects electrons into the MtrC heme wire to enable reduction of Reactive Black 5. The ground state dye is recovered by oxidation of EDTA as sacrificial electron donor. To support this proposal we sought direct evidence for electron transfer from photoreduced MtrC to Reactive Black 5 and this was provided when an excess of the azo dye was added to a solution of photoreduced Ru301-MtrC, Figure 8c. Prior to addition of the azo

dye, that solution displayed a Soret band maximum at 419 nm due to the reduced Fe(II) heme cofactors. Immediately after addition of the azo dye, the Soret band maximum had shifted to 410 nm indicating rapid oxidation of the MtrC hemes through direct electron exchange with Reactive Black 5.

The longevity of photocatalytic performance by Ru657- and Ru301-MtrC was assessed over 8 hours of irradiation with Reactive Black 5 added at the halfway point to return the original azo dye concentration, e.g., Figure 8d and S8. For these conditions the turnover number is 85 Reactive Black 5 molecules reduced per Ru657-MtrC and 73 Reactive Black 5 molecules reduced per Ru301-MtrC. Noting that each Reactive Black 5 contains two azo bonds and therefore 8 electrons for decoloration, this corresponds to 680 and 584 photoenergized electrons directed to azo dye reduction by Ru657-MtrC and Ru301-MtrC respectively. These turnover numbers further confirm photocatalytic, rather than stoichiometric, reduction of Reactive Black 5 by the biohybrid assemblies.

For both Ru-MtrC proteins the time course for reduction of Reactive Black 5 in each 4 hour period is indistinguishable from that in subsequent cycles of irradiation. Thus, there is no evidence for photodamage of the biohybrid assemblies in these experiments. A similar conclusion was reached when the experiment with Ru301-MtrC was extended by storage overnight in the dark at room temperature, addition of Reactive Black 5 to restore the original azo dye concentration and further cycles of irradiation and azo dye addition, Figure S8. Photocatalytic performance on the second day of irradiation was comparable to that on the first day. Over the total 14 hours irradiation, the turnover number was 138 Reactive Black 5 molecules reduced per Ru301-MtrC (1104 photoenergized electrons directed to azo dye reduction). The Ru-MtrC assemblies show no detectable loss of activity after 1 year storage in the dark at -80 ºC.

Figure 8. (over page)

Photocatalytic azo dye reduction by Ru-MtrC biohybrid assemblies.

a) Representative electronic absorbance spectra measured over 1 hour irradiation of Reactive Black 5 (24 μM) with Ru657-MtrC (0.3 μM).

b) Reduction of Reactive Black 5, Methyl Orange and Amaranth, as indicated, for 1 hour irradiation with Ru657-MtrC (red), Ru301-MtrC (teal) and no biohybrid (white). Error bars are standard deviation for 3 measurements and too small to discern for Ru657-MtrC with Methyl Orange. Concentration of azo dye 24 μM and Ru-MtrC 0.3 μM when included.

c) Electronic absorbance spectra of (red) photoreduced Ru301-MtrC (0.1 μM) and (blue) immediately after the addition of Reactive Black 5 to give an azo dye concentration of 19 μM and Ru301-MtrC concentration of 0.08 μM. A spectrum of Reactive Black 5 (blue dots) is shown for reference. Inset: electronic absorbance of photoreduced Ru301-MtrC (red) and immediately after mixing with Reactive Black 5 (black). The electronic absorbance of protein in the mixture is presented as the difference in absorbance of the mixture minus the absorbance of Reactive Black 5. To facilitate spectral comparison the spectrum after addition of Reactive Black 5 has been adjusted to account for sample dilution.

d) Time course of Reactive Black 5 reduction during 8-hour irradiation with Ru657-MtrC (0.35 μM). Arrow indicates the addition of Reactive Black 5 to the cuvette.

All experiments used anaerobic 500 mM EDTA, 20 mM Tris-HCl, 100 mM NaCl, pH 8.5 with irradiation at 450 nm (≈110 W m^{-2}). Data in panels a), b) and c) was collected with a notch filter (Omega Optical 475RB) in place to prevent photoexcitation by the spectrophotometer.

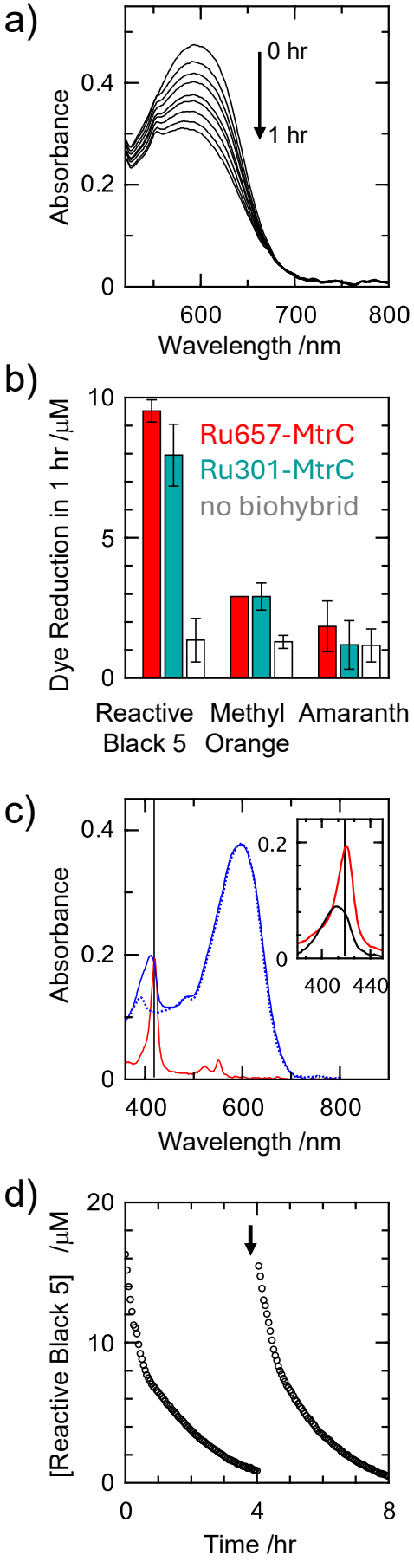
a)
0 hr
1 hr
Absorbance
0
0.2
0.4
600
700
800
Wavelength /nm
b)
Ru657-MtrC
Ru301-MtrC
no biohybrid
Dye Reduction in 1 hr /μM
0
5
10
Reactive Black 5
Methyl Orange
Amaranth
c)
Absorbance
0
0.2
0.4
400
600
800
Wavelength /nm
0
0.2
400
440
d)
[Reactive Black 5] /μM
0
10
20
0
4
8
Time /hr

Rates of photocatalytic Methyl Orange reduction during irradiation in the presence of Ru301-MtrC and Ru657-MtrC were comparable to each other, and approximately 3-fold less than for Reactive Black 5 reduction, Figure 8b. There was little evidence for photocatalytic reduction of Amaranth by the Ru-MtrC assemblies, Figure 8b. Thus, photocatalytic azo dye reduction by the Ru-MtrC biohybrid appears to be independent of the site of Ru(II) dye attachment, i.e., locating the photosensitizer at either end of the heme chain does not interfere with binding and reduction of the azo dyes. It seems more likely that photocatalytic rate is defined by properties of the azo dye. Cyclic voltammetry of the azo dyes under the conditions used for our photochemical investigations, Figure S9, showed the expected irreversible reduction of all three azo dyes. However, the electrochemical potential required for that reduction was dependent on the identity of the azo dye. We quantify this through the potential needed to drive azo dye reduction at a rate that was 2% of the rate at -1 V which for Reactive Black 5 was -200 mV, for Methyl Orange was -258 mV and for Amaranth was -350 mV. Given that MtrC hemes are redox active between approximately 0 and -400 mV it is apparent that the driving force for azo dye reduction decreases in the order Reactive Black 5 > Methyl Orange > Amaranth and that there is very little driving force for the reduction of Amaranth under the experimental conditions. This was corroborated by experiments that introduced the other azo dyes to photoreduced Ru301-MtrC, Figure S10. Following the addition of Methyl Orange, the Soret band maximum moved from 419 nm to lower wavelengths indicating partial oxidation of MtrC over approximately 22 minutes and direct transfer of electrons from the MtrC hemes to Methyl Orange, Figure S10a,b, and after which time there were no further spectral changes. Following the addition of Amaranth, the Soret band maximum remained at 419 nm for at least 60 min, Figure S10c,d. In both experiments there was no irradiation of the sample following addition of the azo dye.

Given that the decrease in driving force for azo dye reduction by MtrC parallels the decrease in rate of Ru-MtrC photocatalysis we consider this property to be the primary determinant of the photocatalytic rate. However, the possibility of contributions to this rate from different substrate binding sites, steric accessibility, or electrostatic interactions cannot be excluded on the basis of the present data.

Conclusions:

Oxidized cytochrome MtrC has been photosensitized by site-selective labeling with a Ru(II)(bipyridine)$_3$ dye at either end of the ten-heme chain that spans the protein. Irradiation of the dye in the Ru-MtrC biohybrid assemblies is followed by charge injection into the heme wire generating a charge separated Ru^{+}-$MtrC^{-}$ state in which the photoenergized electrons reside within MtrC as Fe(II) heme sites. The photoenergized electrons are trapped on MtrC when the oxidized dye is returned to the ground state through reduction by EDTA as sacrificial electron donor and those photoenergized electrons can subsequently transfer to Reactive Black 5 and Methyl Orange such that the Ru-MtrC biohybrids perform photocatalytic reduction of these azo dyes. In the absence of a suitable electron acceptor the photoenergized electrons remain trapped on MtrC for at least 60 minutes.

Azo dye decoloration by our Ru-MtrC biohybrids employs the natural ability of MtrC to catalyze azo dye reduction.[40-44] By contrast, light-driven azo dye decoloration by TiO_2 based systems occurs through oxidation.[64] Photocatalytic oxidation of azo dyes can be driven by reactive oxygen species generated at the surface of aqueous TiO_2 suspensions during irradiation into the band gap with UV-light. Alternatively, photosensitized oxidation (photo-assisted degradation) by irradiation with visible light converts the azo dye to singlet/triplet states that degrade following electron injection into the TiO_2 conduction band.

The Ru-MtrC biohybrid assemblies described here can be considered to operate in a manner analogous to Ru(II)dye-sensitized TiO_2 where photoenergized electrons accumulate in the conduction band to deliver reductive chemical transformations on the TiO_2 surface or via adsorbed redox catalysts that may be synthetic or biological.[11, 45, 46] We anticipate that subsequent decoration of the MtrC protein with an electrocatalyst (natural or synthetic) will allow the Ru-MtrC assembly to drive a wide range of light-driven transformations. Greater rates of photocatalysis should be achieved by identifying Ru(II) dye attachment sites that increase the longevity and/or population of the Ru^{+}-$MtrC^{-}$ charge separated state and/or identifying a more effective system for delivering electrons to the biohybrid assembly.

Funding Sources:

We are grateful to the Science and Technology Facilities Council for access to the ULTRA laser facility (Application 18130011). Funding was from the UK Engineering and Physical Sciences Research Council (EP/M001989/1), UK Biotechnology and Biological Sciences Research Council (BB/S002499/1 and a Doctoral Training Partnership PhD studentship to S.E.H.P.), and a Royal Society of Chemistry Research Enablement Grant (E22-1835404625)

Acknowledgements:

We thank Lucy Marsden and Dr. Simone Payne for assistance with protein purification, and Dr Christopher Hall and Dr Katrin Adamcyzk for help with transient absorbance data collection and analysis.

Author Contributions:

Conceptualization: Julea N. Butt, Jessica H. van Wonderen.

Data curation: Julea N. Butt, Jessica H. van Wonderen

Formal analysis: Jessica H. van Wonderen, Mary E. G. Emmerson, Daisy L. Kent, Samuel H. Piper, Huijie Zhang.

Funding Acquisition: Julea N. Butt, Jessica H. van Wonderen, Lars J. C. Jeuken.

Investigation: Jessica H. van Wonderen, Mary E. G. Emmerson, Daisy L. Kent, Samuel H. Piper, Huijie Zhang.

Project Administration: Julea N. Butt

Resources: Jessica H. van Wonderen, Igor V. Sazanovich (Игорь Сазанович), Michael Towrie, Huijie Zhang.

Supervision: Julea N. Butt, Jessica H. van Wonderen, Stephen R. Meech, Lars J. C. Jeuken

Visualization: Julea N. Butt, Jessica H. van Wonderen, Lars J.C. Jeuken

Writing – Original Draft: Julea N. Butt

Writing – Review and Editing: all authors

Data Availability:

Datasets used for figures are deposited at Figshare (DOI: 10.6084/m9.figshare.31362412)

References:

(1) Morita, I.; Ward, T. R. Recent advances in the design and optimization of artificial metalloenzymes. Curr. Opin. Chem. Biol. 81 (2024) 102508. DOI: 10.1016/j.cbpa.2024.102508.

(2) Jeong, W. J.; Lee, J.; Eom, H.; Song, W. J. A specific guide for metalloenzyme designers: Introduction and evolution of metal-coordination spheres embedded in protein environments. Acc. Chem. Res. 56 (2023) 2416-2425. DOI: 10.1021/acs.accounts.3c00336.

(3) Lovelock, S. L.; Crawshaw, R.; Basler, S.; Levy, C.; Baker, D.; Hilvert, D.; Green, A. P. The road to fully programmable protein catalysis. Nature 606 (2022) 49-58. DOI: 10.1038/s41586-022-04456-z.

(4) de la Torre, D.; Chin, J. W. Reprogramming the genetic code. Nat. Rev. Genet. 22 (2021) 169-184. DOI: 10.1038/s41576-020-00307-7.

(5) Liu, C. C.; Schultz, P. G. Adding new chemistries to the genetic code. Annu. Rev. Biochem. 79 (2010) 413-444. DOI: 10.1146/annurev.biochem.052308.105824.

(6) Lee, K. J.; Kang, D.; Park, H. S. Site-specific labeling of proteins using unnatural amino acids. Mol. Cells 42 (2019) 386-396. DOI: 10.14348/molcells.2019.0078.

(7) Nodling, A. R.; Spear, L. A.; Williams, T. L.; Luk, L. Y. P.; Tsai, Y. H. Using genetically incorporated unnatural amino acids to control protein functions in mammalian cells. Essays Biochem. 63 (2019) 237-266. DOI: 10.1042/EBC20180042.

(8) Eidenschenk, C.; Cheruzel, L. Ru(II)-diimine complexes and cytochrome P450 working hand-in-hand. J. Inorg. Biochem. 213 (2020) 111254. DOI: 10.1016/j.jinorgbio.2020.111254.

(9) Yin, Z.; Ai, J.; Gao, J.; Lin, X.; Lu, F.; Qin, H.-M.; Mao, S. From tradition to innovation: The transition of P450 enzyme catalysis via light-driven electron transfer. ACS Catalysis 15 (2025) 13412–13427. DOI: 10.1021/acscatal.5c02655.

(10) Utschig, L. M.; Mulfort, K. L. Photosynthetic biohybrid systems for solar fuels catalysis. Chem. Commun. 60 (2024) 10642-10654. DOI: 10.1039/d4cc00774c.

(11) Fang, X.; Kalathil, S.; Reisner, E. Semi-biological approaches to solar-to-chemical conversion. Chem. Soc. Rev. 49 (2020) 4926-4952. DOI: 10.1039/c9cs00496c.

(12) Kornienko, N.; Zhang, J. Z.; Sakimoto, K. K.; Yang, P.; Reisner, E. Interfacing nature's catalytic machinery with synthetic materials for semi-artificial photosynthesis. Nat. Nanotechnol. 13 (2018) 890-899. DOI: 10.1038/s41565-018-0251-7.

(13) Zhang, Q.; Liu, X.; Chaker, M.; Ma, D. Advancing graphitic carbon nitride-based photocatalysts toward broadband solar energy harvesting. ACS Mater. Lett. 3 (2021) 663-697. DOI: 10.1021/acsmaterialslett.1c00160.

(14) Wang, P.; Guo, S.; Wang, H. J.; Chen, K. K.; Zhang, N.; Zhang, Z. M.; Lu, T. B. A broadband and strong visible-light-absorbing photosensitizer boosts hydrogen evolution. Nat. Commun. 10 (2019) 3155. DOI: 10.1038/s41467-019-11099-8.

(15) Xiao, K.; Jun, L.; Wang, X.; Hou, T.; Ren, X.; Ying, P.; Ma, Z.; Zeng, C.; Goa, X.; Yu, T.; et al. Panoramic insights into semi-artificial photosynthesis: origin, development, and future perspective. Energy Environ. Sci. 15 (2022) 529-549. DOI: 10.1039/D1EE03094A.

(16) Kissman, E. N.; Sosa, M. B.; Millar, D. C.; Koleski, E. J.; Thevasundaram, K.; Chang, M. C. Y. Expanding chemistry through *in vitro* and *in vivo* biocatalysis. Nature 631 (2024) 37-48. DOI: 10.1038/s41586-024-07506-w.

(17) Breuer, M.; Rosso, K. M.; Blumberger, J.; Butt, J. N. Multi-haem cytochromes in *Shewanella oneidensis* MR-1: structures, functions and opportunities. J. R. Soc. Interface 12 (2015) 20141117. DOI: 10.1098/rsif.2014.1117.

(18) Wang, F.; Gu, Y.; O'Brien, J. P.; Yi, S. M.; Yalcin, S. E.; Srikanth, V.; Shen, C.; Vu, D.; Ing, N. L.; Hochbaum, A. I.; et al. Structure of microbial nanowires reveals stacked hemes that transport electrons over micrometers. Cell 177 (2019) 361-369 e310. DOI: 10.1016/j.cell.2019.03.029.
(19) Wang, F.; Mustafa, K.; Suciu, V.; Joshi, K.; Chan, C. H.; Choi, S.; Su, Z.; Si, D.; Hochbaum, A. I.; Egelman, E. H.; et al. Cryo-EM structure of an extracellular *Geobacter* OmcE cytochrome filament reveals tetrahaem packing. Nat. Microbiol. 7 (2022) 1291-1300. DOI: 10.1038/s41564-022-01159-z.
(20) Clarke, T. A.; Cole, J. A.; Richardson, D. J.; Hemmings, A. M. The crystal structure of the pentahaem *c*-type cytochrome NrfB and characterization of its solution-state interaction with the pentahaem nitrite reductase NrfA. Biochem. J. 406 (2007) 19-30. DOI: 10.1042/BJ20070321.
(21) Jiang, X.; van Wonderen, J. H.; Butt, J. N.; Edwards, M. J.; Clarke, T. A.; Blumberger, J. Which multi-heme protein complex transfers electrons more efficiently? Comparing MtrCAB from *Shewanella* with OmcS from *Geobacter*. J. Phys. Chem. Lett. 11 (2020) 9421-9425. DOI: 10.1021/acs.jpclett.0c02842.
(22) Hwang, E. T.; Sheikh, K.; Orchard, K.; Hojo, D., Radu, V., ; Lee, C.-Y.; Ainsworth, E. V.; Lockwood, C. W. J.; Gross, M.; Adschiri, T.; Reisner, E.; et al. A decaheme cytochrome as a molecular electron conduit in dye-sensitized photoanodes. Adv. Funct. Mater. 25 (2015) 2308-2315.
(23) Ainsworth, E. V.; Lockwood, C. W.; White, G. F.; Hwang, E. T.; Sakai, T.; Gross, M. A.; Richardson, D. J.; Clarke, T. A.; Jeuken, L. J.; Reisner, E.; et al. Photoreduction of *Shewanella oneidensis e*xtracellular cytochromes by organic chromophores and dye-sensitized TiO_2. ChemBioChem 17 (2016) 2324-2333. DOI: 10.1002/cbic.201600339.
(24) Zhang, H. C., C., ; van Wonderen, J. H.; Su, L.; Butt, J. N.; Reisner, E.; Jeuken, L. J. C. Rational design of covalent multiheme cytochrome-carbon dot biohybrids for photoinduced electron transfer. Adv. Funct. Mater. 33 (2023) 2302204. DOI: 10.1002/adfm.202302204.
(25) Zhang, H.; Jaenecke, J.; Bishara-Robertson, I. L.; Casadevall, C.; Redman, H. J.; Winkler, M.; Berggren, G.; Plumere, N.; Butt, J. N.; Reisner, E.; et al. Semiartificial photosynthetic nanoreactors for H_2 generation. J. Am. Chem. Soc. 146 (2024) 34260-34264. DOI: 10.1021/jacs.4c12311.
(26) Piper, S. E. H.; Casadevall, C.; Reisner, E.; Clarke, T. A.; Jeuken, L. J. C.; Gates, A. J.; Butt, J. N. Photocatalytic removal of the greenhouse gas nitrous oxide by liposomal microreactors. Angew. Chem. Int. Ed. 61 (2022) e202210572. DOI: 10.1002/anie.202210572.
(27) Ponomarenko, N. S.; Kokhan, O.; Pokkuluri, P. R.; Mulfort, K. L.; Tiede, D. M. Examination of abiotic cofactor assembly in photosynthetic biomimetics: site-specific stereoselectivity in the conjugation of a ruthenium(II) tris(bipyridine) photosensitizer to a multi-heme protein. Photosynth. Res. 143 (2020) 99-113. DOI: 10.1007/s11120-019-00697-8.
(28) Marzolf, D. R.; McKenzie, A. M.; O'Malley, M. C.; Ponomarenko, N. S.; Swaim, C. M.; Brittain, T. J.; Simmons, N. L.; Pokkuluri, P. R.; Mulfort, K. L.; Tiede, D. M.; et al. Mimicking natural photosynthesis: designing ultrafast photosensitized electron transfer into multiheme cytochrome protein nanowires. Nanomaterials (Basel) 10 (2020). DOI: 10.3390/nano10112143.
(29) Kokhan, O.; Ponomarenko, N. S.; Pokkuluri, P. R.; Schiffer, M.; Mulfort, K. L.; Tiede, D. M. Bidirectional photoinduced electron transfer in Ruthenium(II)-tris-bipyridyl-modified PpcA, a multi-heme *c*-type cytochrome from *Geobacter sulfurreducens*. J. Phys. Chem. B 119 (2015) 7612-7624. DOI: 10.1021/jp511558f.

(30) van Wonderen, J. H.; Hall, C. R.; Jiang, X.; Adamczyk, K.; Carof, A.; Heisler, I.; Piper, S. E. H.; Clarke, T. A.; Watmough, N. J.; Sazanovich, I. V.; et al. Ultrafast light-driven electron transfer in a Ru(II)tris(bipyridine)-labeled multiheme cytochrome. J. Am. Chem. Soc. 141 (2019) 15190-15200. DOI: 10.1021/jacs.9b06858.
(31) van Wonderen, J. H.; Adamczyk, K.; Wu, X.; Jiang, X.; Piper, S. E. H.; Hall, C. R.; Edwards, M. J.; Clarke, T. A.; Zhang, H.; Jeuken, L. J. C.; et al. Nanosecond heme-to-heme electron transfer rates in a multiheme cytochrome nanowire reported by a spectrally unique His/Met-ligated heme. Proc. Natl. Acad. Sci. USA 118 (2021). DOI: 10.1073/pnas.2107939118.
(32) Millett, F.; Durham, B. Design of photoactive ruthenium complexes to study interprotein electron transfer. Biochemistry 41 (2002) 11315-11324. DOI: 10.1021/bi0262956.
(33) van Wonderen, J. H.; Li, D.; Piper, S. E. H.; Lau, C. Y.; Jenner, L. P.; Hall, C. R.; Clarke, T. A.; Watmough, N. J.; Butt, J. N. Photosensitised multiheme cytochromes as light-driven molecular wires and resistors. ChemBioChem 19 (2018) 2206-2215. DOI: 10.1002/cbic.201800313.
(34) Piper, S. E. H.; Edwards, M. J.; van Wonderen, J. H.; Casadevall, C.; Martel, A.; Jeuken, L. J. C.; Reisner, E.; Clarke, T. A.; Butt, J. N. Bespoke biomolecular wires for transmembrane electron transfer: spontaneous assembly of a functionalized multiheme electron conduit. Front. Microbiol. 12 (2021) 714508. DOI: 10.3389/fmicb.2021.714508.
(35) Bafana, A.; Devi, S. S.; Tapan, C. Azo dyes: past, present and the future. Environ. Rev. 19 (2011) 350-371. DOI: 10.1139/a11-018.
(36) Kamenická, B. Chemical degradation of azo dyes using different reducing agents: a review. J. Water Process. Eng. 61 (2024) 105350. DOI: 10.1016/j.jwpe.2024.105350.
(37) Katheresan, V.; Kansedo, J.; Lau, S. Y. Efficiency of various recent wastewater dye removal methods: a review. J. Environ. Chem. Eng. 6 (2018) 4676-4697.
(38) Popli, S.; Patel, U. D. Destruction of azo dyes by anaerobic–aerobic sequential biological treatment: a review. Int. J. Environ. Sci. Technol. 12 (2015) 405-420.
(39) Bhatt, D. K.; Patel, U. D. Photocatalytic degradation of Reactive Black 5 using Ag_3PO_4 under visible light. J. Phys. Chem. Solids. 149 (2021) 109768. DOI: 10.1016/j.jpcs.2020.109768.
(40) Morales-Florez, A.; Lockwood, C. W. J.; Nash, B. W.; Edwards, M. J.; van Wonderen, J. H.; Sachdeva, A.; Butt, J. N.; Clarke, T. A. Extracellular catalysis of environmental substrates by *Shewanella oneidensis* MR-1 occurs via active sites on the C-terminal domains of MtrC. Protein Sci. 34 (2025) e70243. DOI: 10.1002/pro.70243.
(41) Brige, A.; Motte, B.; Borloo, J.; Buysschaert, G.; Devreese, B.; Van Beeumen, J. J. Bacterial decolorization of textile dyes is an extracellular process requiring a multicomponent electron transfer pathway. Microb. Biotechnol. 1 (2008) 40-52. DOI: 10.1111/j.1751-7915.2007.00005.x.
(42) Cai, P. J.; Xiao, X.; He, Y. R.; Li, W. W.; Chu, J.; Wu, C.; He, M. X.; Zhang, Z.; Sheng, G. P.; Lam, M. H.; et al. Anaerobic biodecolorization mechanism of methyl orange by *Shewanella oneidensis* MR-1. Appl. Microbiol. Biotechnol. 93 (2012) 1769-1776. DOI: 10.1007/s00253-011-3508-8.
(43) Pearce, C. I.; Christie, R.; Boothman, C.; von Canstein, H.; Guthrie, J. T.; Lloyd, J. R. Reactive azo dye reduction by *Shewanella* strain J18 143. Biotechnol. Bioeng. 95 (2006) 692-703. DOI: 10.1002/bit.21021.
(44) Cao, D. M.; Xiao, X.; Wu, Y. M.; Ma, X. B.; Wang, M. N.; Wu, Y. Y.; Du, D. L. Role of electricity production in the anaerobic decolorization of dye mixture by exoelectrogenic bacterium *Shewanella oneidensis* MR-1. Bioresour. Technol. 136 (2013) 176-181. DOI: 10.1016/j.biortech.2013.02.083.

(45) Watanabe, M. Dye-sensitized photocatalyst for effective water splitting catalyst. Sci. Technol. Adv. Mater. 18 (2017) 705-723. DOI: 10.1080/14686996.2017.1375376.
(46) Youngblood, W. J.; Lee, S. H.; Maeda, K.; Mallouk, T. E. Visible light water splitting using dye-sensitized oxide semiconductors. Acc. Chem. Res. 42 (2009) 1966-1973. DOI: 10.1021/ar9002398.
(47) Lockwood, C. W. J.; van Wonderen, J. H.; Edwards, M. J.; Piper, S. E. H.; White, G. F.; Newton-Payne, S.; Richardson, D. J.; Clarke, T. A.; Butt, J. N. Membrane-spanning electron transfer proteins from electrogenic bacteria: Production and investigation. Methods Enzymol. 613 (2018) 257-275. DOI: 10.1016/bs.mie.2018.10.011.
(48) Kalyanasundaram, K. Photophysics, photochemistry and solar-energy conversion with tris(bipyridyl)Ruthenium(II) and its analogs. Coord. Chem. Rev. 45 (1982) 159-244. DOI: 10.1016/0010-8545(82)85003-0.
(49) Yang, F.; Bogdanov, B.; Strittmatter, E. F.; Vilkov, A. N.; Gritsenko, M.; Shi, L.; Elias, D. A.; Ni, S.; Romine, M.; Pasa-Tolic, L.; et al. Characterization of purified *c*-type heme-containing peptides and identification of *c*-type heme-attachment sites in *Shewanella oneidenis* cytochromes using mass spectrometry. J. Proteome Res. 4 (2005) 846-854. DOI: 10.1021/pr0497475.
(50) Blumel, S.; Knackmuss, H. J.; Stolz, A. Molecular cloning and characterization of the gene coding for the aerobic azoreductase from *Xenophilus azovorans* KF46F. Appl. Environ. Microbiol. 68 (2002) 3948-3955. DOI: 10.1128/AEM.68.8.3948-3955.2002.
(51) Saraswati, T. E.; Astuti, A. R.; Rismana, N. Quantitative analysis by UV-Vis absorption spectroscopy of amino groups attached to the surface of carbon-based nanoparticles. IOP Conf. Ser.: Mater. Sci. Eng. 333 (2018) 012027. DOI: 10.1088/1757-899X/333/1/012027.
(52) Bissaro, B.; Kodama, S.; Nishiuchi, T.; Diaz-Rovira, A. M.; Hage, H.; Ribeaucourt, D.; Haon, M.; Grisel, S.; Simaan, A. J.; Beisson, F.; et al. Tandem metalloenzymes gate plant cell entry by pathogenic fungi. Sci. Adv. 8 (2022) eade9982. DOI: 10.1126/sciadv.ade9982.
(53) Kurth, J. M.; Dahl, C.; Butt, J. N. Catalytic protein film electrochemistry provides a direct measure of the tetrathionate/thiosulfate reduction potential. J. Am. Chem. Soc. 137 (2015) 13232-13235. DOI: 10.1021/jacs.5b08291.
(54) Guerois, R.; Nielsen, J. E.; Serrano, L. Predicting changes in the stability of proteins and protein complexes: a study of more than 1000 mutations. J. Mol. Biol. 320 (2002) 369-387. DOI: 10.1016/S0022-2836(02)00442-4.
(55) Krieger, E.; Vriend, G. Models@Home: distributed computing in bioinformatics using a screensaver based approach. Bioinformatics 18 (2002) 315-318. DOI: 10.1093/bioinformatics/18.2.315.
(56) Schymkowitz, J.; Borg, J.; Stricher, F.; Nys, R.; Rousseau, F.; Serrano, L. The FoldX web server: an online force field. Nucleic Acids Res. 33 (2005) W382-388. DOI: 10.1093/nar/gki387.
(57) Van Durme, J.; Delgado, J.; Stricher, F.; Serrano, L.; Schymkowitz, J.; Rousseau, F. A graphical interface for the FoldX forcefield. Bioinformatics 27 (2011) 1711-1712. DOI: 10.1093/bioinformatics/btr254.
(58) Hartshorne, R. S.; Jepson, B. N.; Clarke, T. A.; Field, S. J.; Fredrickson, J.; Zachara, J.; Shi, L.; Butt, J. N.; Richardson, D. J. Characterization of *Shewanella oneidensis* MtrC: a cell-surface decaheme cytochrome involved in respiratory electron transport to extracellular electron acceptors. J. Biol. Inorg. Chem. 12 (2007) 1083-1094. DOI: 10.1007/s00775-007-0278-y.
(59) Edwards, M. J.; White, G. F.; Norman, M.; Tome-Fernandez, A.; Ainsworth, E.; Shi, L.; Fredrickson, J. K.; Zachara, J. M.; Butt, J. N.; Richardson, D. J.; et al. Redox linked

flavin sites in extracellular decaheme proteins involved in microbe-mineral electron transfer. Sci. Rep. 5 (2015) 11677. DOI: 10.1038/srep11677.
(60) Juris, A.; Balzani, V.; Barigelletti, F.; Campagna, S.; Belser, P.; von Zelewsky, A. Ru(II) polypyridine complexes: photophysics, photochemistry, electrochemistry, and chemiluminescence. Coord. Chem. Rev. 84 (1988) 85-277. DOI: 10.1016/0010-8545(88)80032-8.
(61) Wang, L.; Ashford, D. L.; Thompson, D. W.; Meyer, T. J.; Papanikolas, J. M. Watching photoactivation in a Ru(II) chromophore-catalyst assembly on TiO_2 by ultrafast spectroscopy. J. Phys. Chem. C 117 (2013) 24250-24258. DOI: 10.1021/jp410571x.
(62) Bettis, S. E.; Hanson, K.; Wang, L.; Gish, M. K.; Concepcion, J. J.; Fang, Z.; Meyer, T. J.; Papanikolas, J. M. Photophysical characterization of a chromophore/water oxidation catalyst containing a layer-by-layer assembly on nanocrystalline TiO_2 using ultrafast spectroscopy. J. Phys. Chem. A 118 (2014) 10301-10308. DOI: 10.1021/jp411139j.
(63) Jiang, X.; Burger, B.; Gajdos, F.; Bortolotti, C.; Futera, Z.; Breuer, M.; Blumberger, J. Kinetics of trifurcated electron flow in the decaheme bacterial proteins MtrC and MtrF. Proc. Natl. Acad. Sci. USA 116 (2019) 3425-3430. DOI: 10.1073/pnas.1818003116.
(64) Konstantinou, I. K., Albanis, T. A. TiO_2-assisted photocatalytic degradation of azo dyes in aqueous solution: kinetic and mechanistic investigations: a review. Appl. Catal. B: Environ. 49 (2004) 1-14. DOI: 10.1016/j.apcatb.2003.11.010